Available online at www.sciencedirect.com
ScienceDirect
Thermochimica Acta 469 (2008) 104–108
thermochimica acta
www.elsevier.com/locate/tca

Design of glass–ceramic complex microstructure with using onset point of crystallization in differential thermal analysis

Seongjin Hwang [a], Jinho Kim [a], Hyo-Soon Shin [b], Jong-Hee Kim [b], Hyungsun Kim [a,*]

[a] *School of Materials Engineering, Inha University, 253 Younghyun-dong, Nam-gu, Incheon 402-751, Republic of Korea*
[b] *Fusion Technology Division, KICET, 233-5 Gasan-Dong, Guemcheon-gu, Seoul 153-801, Republic of Korea*

Received 12 November 2007; received in revised form 14 January 2008; accepted 14 January 2008
Available online 19 January 2008

Abstract

Two types of frits with different compositions were used to develop a high strength substrate in electronic packaging using a low temperature co-fired ceramic process. In order to reveal the crystallization stage during heating to approximately 900 °C, a glass–ceramic consisting of the two types of frits, which had been crystallized to diopside and anorthite after firing, was tested at different mixing ratios of the frits. The exothermal peaks deconvoluted by a Gauss function in the differential thermal analysis curves were used to determine the onset point of crystallization of diopside or anorthite. The onset points of crystallization were affected by the mixing ratio of the frits, and the microstructure of the glass–ceramic depended on the onset point of crystallization. It was found that when multicrystalline phases appear in the microstructure, the resulting complex microstructure could be predicted from the onset point of crystallization obtained by differential thermal analysis.

Keywords: Low temperature co-fired ceramic (LTCC); Glass–ceramic; Diopside; Anorthite; Onset point of crystallization

1. Introduction

Substrates for the system-on-package require several properties; a low coefficient of thermal expansion (CTE), high strength, low dielectric constants, high quality factor and a stable temperature coefficient due to the high reliability and high signal propagation speed in the electronic industry [1,2]. The properties of many ceramic packaging systems with potential substrate materials have been reported [1,2]. The low temperature co-fired ceramic (LTCC) substrate is focused on the system-on-package due to the possibility of firing with high conductive electrodes, such as silver and copper (<900 °C).

LTCC substrates have been developed using a number of glass matrix/ceramic composites with the aim of improving the properties of packaging devices: glass matrix–Al_2O_3, cordierite ($2MgO–2Al_2O_3–5SiO_2$) fillers [3], glass matrix–AlN filler [4], glass–ceramic matrix–AlN filler [5] and glass–ceramic matrix–Al_2O_3 filler [6,7]. Several studies on the applications of glass–ceramics based on the diopside and anorthite system have been carried out [4,8]. However, the increasing requirements for high performance substrates have highlighted the need to optimize the properties of glass–ceramics, such as the strength and reliability which are related to high densification, microstructure and fabrication factors in LTCC substrates. As a further improvement in the substrate properties, we recently reported that high densification and strength of LTCC substrates could be achieved using a mixture of the two frits with the anorthite and diopside compositions, and alumina [9]. Unfortunately, there is insufficient information to explain the crystallization phenomena derived from the two different glass powder compositions through glass sintering and crystallization during firing.

This study examined the mechanism that governs the material behavior with the microstructure using a mixture of two frits with two different crystal phases (anorthite and diopside) after firing at 900 °C. The microstructure of the complex glass–ceramics was investigated by thermal analysis. In particular, differential thermal analysis and X-ray diffraction were used to confirm the crystallites in the glass–ceramics based on the DTA analysis.

2. Experimental procedure

The raw materials used for the glass frits were high purity $55SiO_2–7Al_2O_3–23CaO–10MgO–3Na_2O–2Fe_2O_3$ (*CMS*, in

* Corresponding author. Tel.: +82 2 860 7545; fax: +82 2 864 3730.
E-mail address: kimhs@inha.ac.kr (H. Kim).

0040-6031/$ – see front matter © 2008 Elsevier B.V. All rights reserved.
doi:10.1016/j.tca.2008.01.011

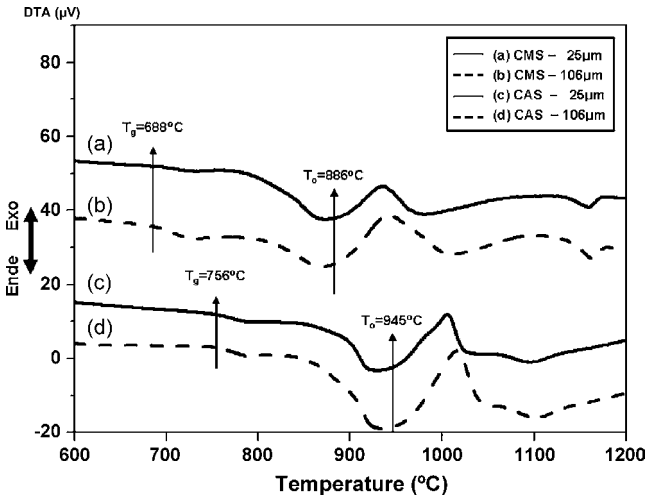

Fig. 1. DTA curves of the *CMS* and *CAS* frits with fine and coarse powders with increasing temperature at a heating rate of 10 °C/min: (a) *CMS* frit-25 μm, (b) *CMS* frit-106 μm, (c) *CAS* frit-25 μm and (d) *CAS* frit-106 μm.

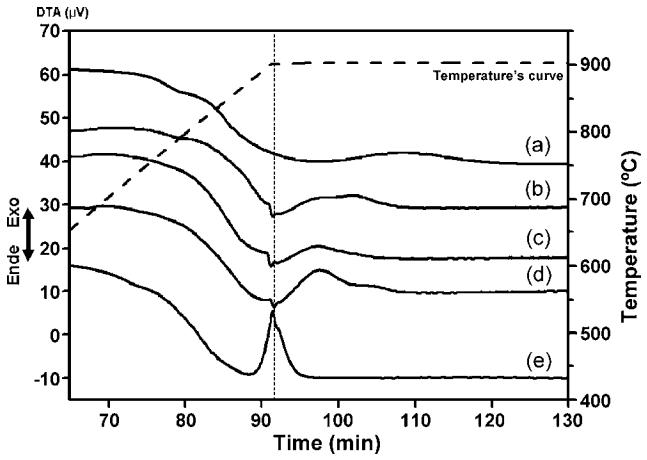

Fig. 2. DTA curves of the powders with the heating profile (heating rate of 10 °C/min, holding at 900 °C for 1 h); the powders have a different mixture: x *CMS* frit and $(1-x)$ *CAS* frit (a) $x=0$, (b) $x=0.1$, (c) $x=0.3$, (d) $x=0.5$ and (e) $x=1$ (wt%).

mol.%) and $50SiO_2$–$22Al_2O_3$–$23CaO$–$5B_2O_3$ (*CAS*, in mol.%) (Aldrich, USA). The batches were melted in a platinum crucible at 1500 °C for 3 h. The molten glasses were poured quickly and quenched on a ribbon roller. The glass cullets were then pulverized using a planetary mono mill (Pulverisette5, Fritsch, Germany) for 7 h. The (x) *CMS* frit and $(1-x)$ *CAS* frit ($x=0$, 0.1, 0.3, 0.5, 1) were mixed using a ball mill for 24 h and dried at 130 °C for 24 h. The mixture powders were dried, and pellets

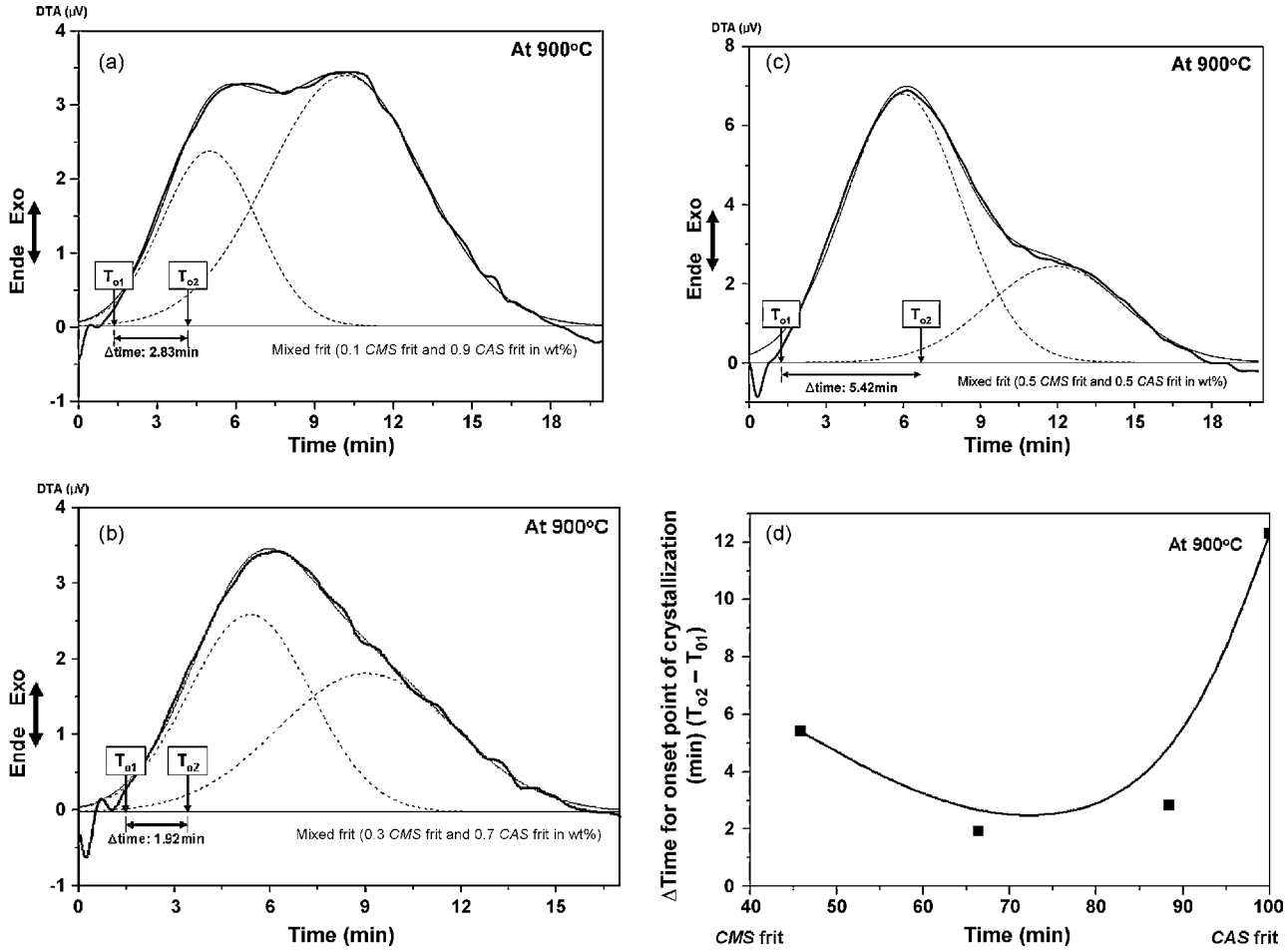

Fig. 3. Isothermal DTA curves at 900 °C and the deconvoluted exothermal peaks using the Gauss function for powders consisting of x *CMS* frit and $(1-x)$ *CAS* frit (a) $x=0.1$, (b) $x=0.3$, (c) $x=0.5$ in wt% and (d) difference of the time, onset point of crystallization between T_{01} and T_{02} at 900 °C with the two types of frit in vol%.

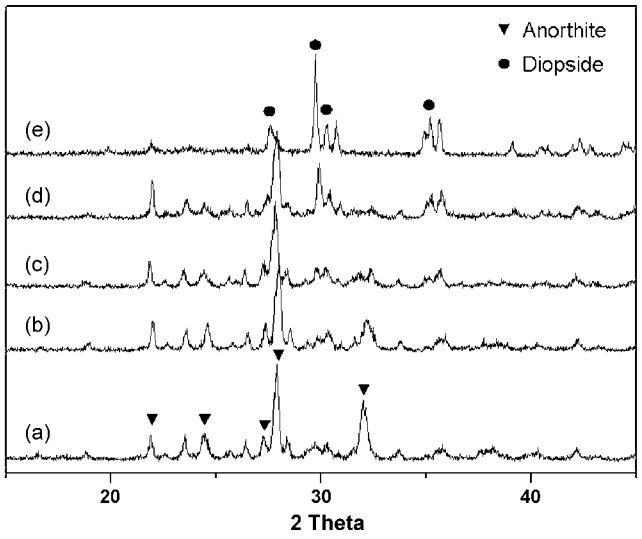

Fig. 4. X-ray diffraction patterns of the frits containing the materials: x *CMS* frit and $(1-x)$ *CAS* frit (a) $x=0$, (b) $x=0.1$, (c) $x=0.3$, (d) $x=0.5$ and (e) $x=1$ in wt% after firing at 900 °C for 1 h.

(20 mm in diameter) were made by uniaxial pressing (62 MPa). The pellets were sintered at 900 °C for 1 h at a heating rate of 10 °C/min.

The particle size distribution of the powder was determined using a particle size analyzer (LS230 & N4PLUS, Coulter Corporation, USA). The glass transition temperature (T_g) and onset point of crystallization (T_c) were determined using a differential thermal analyzer (DTA, TG 8120, Rigaku Co, Japan) at a heating rate of 10 °C/min. The microstructures of the sintered pellets were characterized by scanning electron microscopy (SEM, HITACHI, Japan), and the phases of the glasses, sintered and quenched samples were identified by X-ray powder diffraction (XRD, Rigaku DMAX 2500, Japan).

3. Results and discussion

The *CMS* and CAS frits have significantly different thermal properties. These include the glass transition temperature (T_g) and onset point of crystallization (T_0), as shown in Fig. 1. The T_g and T_0 for the *CMS* frits were observed at 688 and 886 °C, respectively. The T_g (756 °C) and T_0 (945 °C) for the *CAS* frits were higher than that of the *CMS* frits. A comparison of the T_g and T_0 between the fine and coarse powders showed that each of the *CMS* and *CAS* frits have the same T_g and T_0. Therefore, crystallization of the *CMS* and *CAS* frits in each of the glass systems was the result of bulk crystallization rather than surface crystallization [10,11].

When the temperature was held at 900 °C, the onset point of crystallization appeared within 30 min in the frits without the *CMS* frit, which had crystallized before reaching 900 °C. However, the DTA results of the mixed frits showed asymmetrical curves (Fig. 2). The DTA curves of the exothermal peaks should be asymmetrical considering that the two crystallization processes in the mixed frits occur concurrently. In order to show the hidden onset point of crystallization, the asymmetrical DTA curves of the mixed frits were deconvoluted using a Gauss function for two peaks, respectively (Fig. 3). The T_{02} of the mixed frits shown in Fig. 3 was observed in the asymmetrical DTA

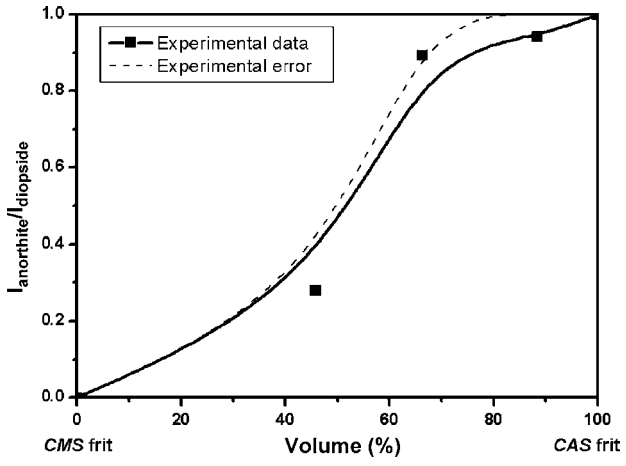

Fig. 5. Normalized ratio of the XRD intensity of the anorthite and diopside peaks determined from the frits after firing at 900 °C for 1 h.

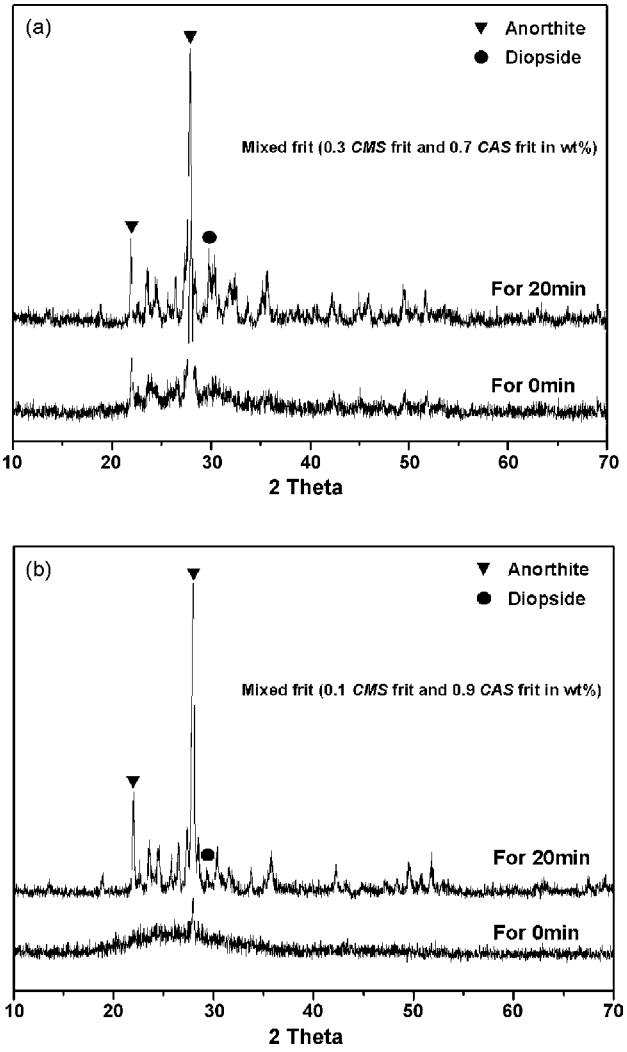

Fig. 6. X-ray diffraction patterns of the mixed frits fired at 900 °C for 0 and 20 min: x *CMS* frit and $(1-x)$ *CAS* frit (a) $x=0.3$, (b) $x=0.1$ in wt%.

curves using this method. Fig. 3 (d) shows the difference between the time for T_{02} and T_{01} as a function of the ratios of the frits in vol%. The T_{02} was activated by adding up to 35 vol% of the *CMS* frit. The time for T_{02} in the glass–ceramic was influenced by the *CMS* and *CAS* frit ratios.

After firing at 900 °C for 1 h, the *CAS* and *CMS* frits were transformed into a glass–ceramic containing anorthite and diopside, respectively (Fig. 4). This shows that the onset points of crystallization with the *CAS* and *CMS* frits were assigned to the formation of the anorthite and diopside. Moreover, the XRD patterns of the mixed frits fired at 900 °C for 1 h were similar to anorthite despite the inclusion of the *CMS* frit. However, a mixed frit containing 0.5 wt% *CMS* frit and 0.5 wt% *CAS* frit showed the peaks for diopside after firing (Fig. 4(d)). This suggests that the mixed frits have two crystal phases after firing at 900 °C; anorthite and diopside from the *CMS* and *CAS* frits, respectively. Moreover, the T_{01} and T_{02} shown in Fig. 3 indicate the time for the formation of diopside and anorthite, respectively at 900 °C. The main peaks for diopside were difficult to determine in the XRD pattern shown in Fig. 4 (b) and (c). The reasons are that the content of the *CMS* frit was smaller than that of the *CAS* frit and the *CMS* frit can crystallize at that time [12,13].

Considering that the intensity of the strong peaks for both crystalline phases corresponds to the contents of the crystal phases, the relative ratio between the anorthite and diopside content can be plotted as a function of the frit ratios, as shown in Fig. 5 [11]. The experimental error resulted from the calculation using various and shifted peaks in Fig. 4. The decrease in anorthite was attributed to a decrease in the *CAS* frit from the normalized ratio of the XRD intensity of the anorthite and diopside peaks determined from the frits after firing at 900 °C for 1 h. Furthermore, there is a critical point in the ratio between the anorthite and diopside content. The addition of 40 vol% of the *CMS* frit to the mixture of frits fired at 900 °C for 1 h made a significant contribution to decreasing the anorthite content in the glass–ceramic.

Isothermal DTA curves of the mixed frits show that the mixed frit containing 0.3 *CMS* frit and 0.7 *CAS* frit in wt % crystallized

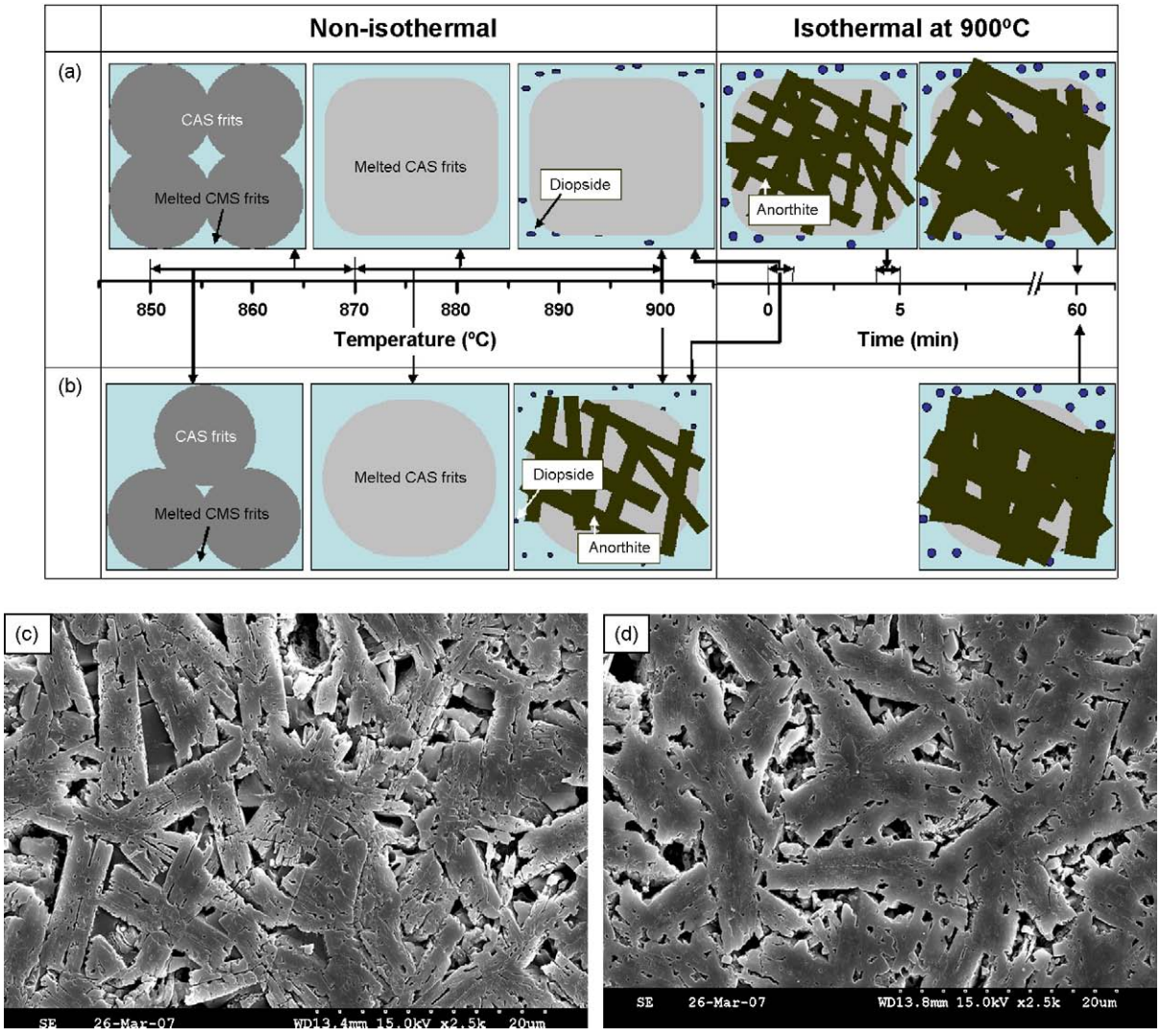

Fig. 7. Schematic model of the microstructure of the mixed frits as a function of temperature and time: x *CMS* frit and $(1-x)$ *CAS* frit (a) $x = 0.1$ and (b) $x = 0.3$ in wt%, SEM images of the sintered bodies at 900 °C for 1 h etched by 0.5% HNO_3; x *CMS* frit and $(1-x)$ *CAS* frit (c) $x = 0.1$ and (d) $x = 0.3$ in wt%.

into diopside and anorthite at 900 °C after 3.5 min. This was confirmed by XRD, as shown in Fig. 6(a). However, crystallization of the mixed frit fired at 900 °C occurred immediately, which might be due to experimental error. The XRD patterns of the mixed frit, which was fired at 900 °C for 20 min, show two crystalline phases, anorthite and diopside. The anorthite and diopside show significantly different XRD intensities, which suggests that anorthite crystal growth begins within 20 min.

Fortunately, there was no noticeable crystal phase in the XRD patterns of the mixed frit containing 0.1 *CMS* frit and 0.9 *CAS* frit fired at 900 °C for 0 min (Fig. 6b). This agrees with the isothermal DTA curve that the onset point of crystallization (T_{02}), i.e. the formation of anorthite, appears after 4.33 min. Therefore, the mixed frit containing *CMS* and *CAS* frits (in wt%) should be associated with the onset point of crystallization.

Fig. 7 shows a schematic model of the effect of the onset point of crystallization with the microstructure based on the present results. The mixing ratio of the frits contributed to the changes in T_{02}. In addition, the anorthite content in the frits fired at 900 °C for 1 h was dependent on the *CMS*: *CAS* ratio. With increasing temperature, the *CMS* frit transformed to a glass matrix in the mixed frits due to the lower T_g than the *CAS* frit, which had melted into the glass matrix. The melted *CAS* frit affects the crystallization of diopside. In the melted frits, there are chemical reactions between the melted frits, which results in the later formation of diopside compared with the *CMS* frit. After the formation of diopside, the residual glass from the melted *CMS* frit contributes to the formation of anorthite. Moreover, crystal growth occurs after the formation of anorthite and diopside. The size of the crystals is dependent on the rate of crystal growth. If the rate of crystal growth is the same at any condition, the size of the crystals would be determined by the time of crystallization. Fig. 7(c) and (d) shows that the microstructure of the fired frit at 900 °C for 1 h with the ratio of the frits is the same as that shown in the schematic model.

DTA, XRD and SEM showed that the microstructure of the glass–ceramic was dependent on the onset point of crystallization. Furthermore, the onset points of crystallization could be determined using a deconvoluted method with a Gauss function. Therefore, thermal analysis can be used to predict the microstructure of the glass–ceramic in LTCC materials with a complex microstructure.

4. Conclusion

Multicrystalline phases for high strength LTCC materials were examined by DTA, XRD and SEM. Based on these results, an invisible onset point of crystallization was observed in the asymmetrical DTA curves using a deconvoluting method with a Gauss function. We propose a schematic model for the effect of the onset point of crystallization on a complex microstructure of two frits, which had crystallized to anorthite and diopside. This model can predict the complex microstructure in high strength LTCC materials using thermal analysis.

Acknowledgements

This work is financially partially supported by the Ministry of Education and Human Resources Development (MOE), the Ministry of Commerce, Industry and Energy (MOCIE) and the Ministry of Labor (MOLAB) through the fostering project of the Lab of Excellency and was supported by the IT R&D program of MIC/IITA. [2006-s055-02, Ceramic Material and Process for High Integrated Module].

References

[1] J.L. Sprague, IEEE Trans. Comp. Hybrids Manuf. Technol. 13 (1990) 390–396.
[2] R.R. Tummala, J. Am. Ceram. Soc. 74 (1991) 895–908.
[3] C.E. Borsa, R.J. Brook, in: H. Hausner, G.L. Messing, S.-I. Hirano (Eds.), Ceramic Transactions, vol. 51, Ceramic Processing and Science, American Ceramic Society, Westerville, OH, 1995, p. 681.
[4] C.L. Lo, J.G. Duh, J. Mater. Sci. 38 (2003) 693.
[5] G.H. Chen, X.Y. Liu, J. Mater. Process. Technol. 190 (2007) 77–80.
[6] Korea Patent 10-2006-0119121, 2006.
[7] Japan Patent 2004-312156(P2004-312156), 2005.
[8] K. Hayshi, Y. Nishoka, Y. Okamto, J. Ceram. Soc. Jpn. 95 (1990) 801–805.
[9] V.M.F. Marques, D.U. Tulyaganov, S. Agathopoulos, V.K. Gataullin, G.P. Kothiyal, J.M.F. Ferreira, J. Eur. Ceram. Soc. 26 (2006) 2503–2510.
[10] B.H. Jung, S.J. Hwang, H.S. Kim, J. Eur. Ceram. Soc. 25 (2005) 3187–3193.
[11] H. Kim, W. Choi, J. Eur. Ceram. Soc. 24 (2004) 2103–2111.
[12] F.H. Chung, D.K. Smith, Industrial Applications of X-ray Diffraction, Marcel Dekker Inc., New York, 2000.
[13] A. Karamanov, M. Pelino, J. Eur. Ceram. Soc. 19 (1999) 649–654.